Thickness Dependence of Structural, Electrical and Optical Properties of Sputter Deposited Indium Tin Oxide Films

S. Sivaranjani[1], V. Malathy[2], J. Joseph Prince[1], B. Subramanian[4], T. Balasubramanian[2], C. Sanjeeviraja[3], M. Jayachandran[4], and V. Swaminathan[5, *]

[1]*Department of Physics, Anna University, Trichy 620 024, India*
[2]*Department of Physics, National Institute of Technology, Trichy 620 015, India*
[3]*School of Physics, Alagappa University, Karaikudi 630 003, India*
[4]*ECMS Division, Central Electrochemical Research Institute*
(Council of Scientific and Industrial Research), Karaikudi 630 006, India
[5]*School of Materials Science and Engineering, Nanyang Technological University, Singapore 639 798*

We report the results on low resistance indium tin oxide (ITO) thin films produced by r.f magnetron sputtering of a ceramic oxide target under Ar gas atmosphere. Thickness of the deposition has been tailor made from 0.74 μm to 2.58 μm by adjusting the time; the deposited films were characterized by XRD, TEM, electrical, optical and AFM studies. X-ray diffraction studies confirmed the presence of the ITO cubic phase with preferred orientation on (222) and (400) occurred for the films with thickness greater than 1.29 μm. It was observed that average grain size increases from 10.5 nm to 34.4 nm with increasing film thickness from 0.84 μm to 2.58 μm. The lowest sheet resistance and the lowest resistivity were measured at 1.68 μm and the corresponding values are found to be 12.36 Ω/square and 2.077×10^{-3} Ω cm. The carrier concentration and mobility were calculated for 1.68 μm ITO thin films. The variation of refractive index and extinction coefficient with wavelength for the film deposited with 1.68 μm thickness were studied. It shows a high refractive index value of 1.92 at 550 nm which is in agreement with the reported value of 1.86 for the ITO films deposited by r.f magnetron sputtering. In the present work, ITO thin films possessing highly compact, void free and fully crystallized structure have been produced with an optimum thickness of 1.68 μm, which can be suitably and selectively used for solar cells, charge coupled devices and LCD applications.

1. INTRODUCTION

Tin (Sn) doped indium oxide, commonly called as ITO, is one of the most popular transparent semiconductor compounds and has been intensively studied in recent years. This is a n-type semiconductor with a wide band gap (direct band gap energy of 3.6 eV) which exhibits a low electrical resistivity ($<10^{-4}$ Ω cm)[1,2] and high optical transmittance (85–90%) in the visible region. The vital material properties possessed by ITO thin films are mechanical hardness, high transparency and chemical inertness, which are highly needed for various applications.

The ITO films have been produced using different deposition techniques such as reactive thermal evaporation (RTE),[3] chemical vapour deposition (CVD),[4] electron beam evaporation,[5] spray pyrolysis[6] and sputtering (with radio frequency),[7] direct current (d.c)[8] or magnetron assisted.[9] These films have been developed

aiming their applications as electric contacts and anti reflection coatings in a large variety of devices such as solar cells,[10] photo diodes,[11] image sensors,[12] liquid crystal displays[13] and charge coupled devices.[14]

The properties of ITO films are strongly dependent on the deposition conditions, most significantly on the substrate temperature and the distance between the target and the substrate. There have been a lot of reports on dependence between these parameters. Some researchers have also studied the effect of films thickness on the properties of ITO films, e.g., Kim et al.[15] reported on the properties of ITO thin films (40 nm–870 nm) grown by pulsed laser deposition and Guittoum et al[16] studied the influence of the film's thickness on the physical properties of ITO films prepared by d.c. diode sputtering at low substrate temperature (80 °C).

In In_2O_3 films, carriers are generated by the oxygen vacancies.[17,18] In ITO films, the contribution of carriers to the conduction band occur either through creation of oxygen

*Author to whom correspondence should be addressed.

vacancies $[V_0]$ or substitutionally four–valent Sn atoms. The creation a V_0 supplies a maximum of 2 electrons, while the substitution of an In atom with Sn atom provides an electron for the conduction process. Both conditions are true for crystalline ITO films.

In this article, we report on an extensive study of the effect of film thickness on the growth and the microstructural, electrical, optical and surface morphological properties of ITO films deposited with different thickness by r.f. magnetron sputtering by varying time of deposition.

2. EXPERIMENTAL DETAILS

ITO thin films were deposited on quartz substrates by r.f. sputtering deposition method using 13.56 MHz radio frequency magnetron sputtering system with 99.99% tin doped indium oxide (90:10 at %) ceramic target. The base pressure of the deposition chamber was 10^{-6} torr and the working pressure was kept at 5×10^{-3} torr under pure argon ambient. Sputtering was carried out by keeping the target to substrate distance constant at about 8 cm through out the experiment. The substrate temperature and the r.f power were kept constant through out the deposition at 150 °C and 250 W respectively. The deposition was carried out for 10–30 min to obtain ITO films of different thickness values ranging from 0.74 μm to 2.58 μm. These films were obtained in the atmosphere of pure Ar gas and the effect of thickness on the structural, electrical, optical and morphological properties were studied.

The quartz substrates were first cleaned by a detergent, washed with distilled water, kept in freshly prepared hot chromic acid for 1 hour, again thoroughly cleaned with distilled water and finally subjected to ultrasonic cleaning for 1 hour. Film thickness was measured by the Stylus Profilometer (Mitutoyo). The optical transmittance measurements were made in the wavelength range 300–1100 nm using a Hitachi-330 UV-Vis-NIR spectrophotometer. X-ray diffraction (XRD) measurements were carried out with X'pert Pro PANalytical using CuKα radiation ($\lambda = 1.5406$ Å) to study the crystalline properties of the films. Electrical properties were measured by a Four probe set up model DEP-02 (Scientific Equipment) DC power supply. Hall mobility and carrier concentration were calculated from the Hall voltage measured by the Vander Pauw method with a Ecopia HMS 3000 Hall constant measurement system. Surface morphology of the films was studied by Nanoscope E-3138j AFM/STM Molecular Imaging system atomic force microscope. TEM image and selected area electron diffraction (SAED) pattern were recorded using a JEOL 2010 Transmission Electron Microscope instrument.

3. RESULTS AND DISCUSSION

3.1. Structural Analysis by XRD

The analysed crystal structures conducted from X-ray diffraction patterns for various ITO samples deposited with thickness values 0.74, 0.84, 1.29, 1.39, 1.68 and 2.58 μm are shown in (Figs. 1(a–f)). On all the samples, the cubic bixbyite structure of indium oxide (JCPDS 6–0416) without any indication of crystalline SnO_2 as an additional phase was registered. The XRD peaks of all samples are confirmed to correspond well to In_2O_3 structure by comparing them with the standard XRD data base[19] and no peaks from other materials are observed. The broad and
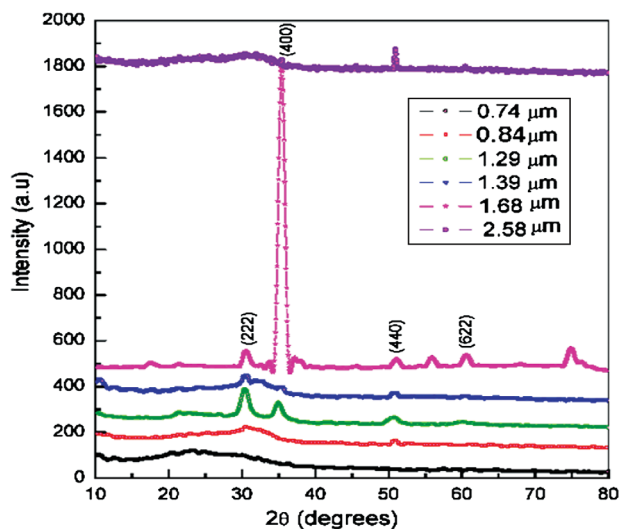
Fig. 1. X-ray diffraction patterns for various ITO samples deposited with thickness in the range from 0.74 μm to 2.58 μm.

weak diffraction region observed from the diffraction pattern of the ITO film with 0.74 μm thickness, as is seen from (Fig. 1(a)), was regarded as the contribution of the amorphous-like structure.

However, in an amorphous state, it has been reported that the presence of Sn atoms in the ITO films does not contribute free carriers to the conduction band; rather they act as scattering centres in the films.[20, 21] In the case of ITO film with 0.86 μm, as is seen from (Fig. 1(b)), the most intensive diffraction pattern appears at 50.8°. Besides, main diffraction patterns are detected at 30.9° and 59.9°. These peaks are coincident with the diffraction from (440), (222) and (622) orientation of cubic crystalline ITO[22, 23] respectively. Therefore, the synthesised ITO film at 0.86 μm seems to be a well crystallized cubic structure with a crystallite size of 10.5 nm.

The X-ray diffraction pattern of the film deposited with 1.29 μm thickness also exhibits peaks only from the cubic (bixbyite) structure of indium oxide.

In the case of ITO films with 1.29 μm and 1.39 μm thickness, as is seen in from (Figs. 1(c, d)), the three most intensive Bragg peaks −(222), (400) and (440) with an average crystallite size of 13.6 and 30.1 nm were obtained respectively. This confirms the crystallinity of the ITO samples and proves the presence of Cubic In_2O_3 lattice plane (222) with 2.927 Å, (400) with 2.58 Å and (440) with 1.789 Å for the sample with 1.29 μm thickness; for the sample with 1.39 μm, lattice plane (222) with 2.933 Å, (400) with 2.54 Å and (440) with 1.796 Å.

In Figure 1(e), for the ITO film deposited with 1.68 μm, a sharp peak only for (400) orientation as well as small and narrow peaks for (222), (440) and (125) orientations could be found. The reason for (400) preferred orientation is that the concentration of oxygen vacancies in the ITO film at high temperature sputtering is higher than that of room temperature sputtering because of the reduced sticking coefficient of oxygen at higher temperatures. According to the literature, the predominant orientation changes from (222) to (400) as the oxygen incorporation in the structure decreases or the deposition rate increases.[24–26] On the other hand, the change in orientation from (222) to (400) can also influence the deposition rate because (222) oriented grains are less resistant against r.f sputtering than (400) grains.[24–27]

Besides, an increase of the (400) texture with the film thickness has been also observed for ITO layers deposited by the pulsed laser deposition[28] or by the spray pyrolysis[29] techniques. This coincidence in the structures of ITO films deposited by different methods indicates that these layers grow with a common mechanism. Therefore crystalline ITO deposited with 1.68 μm typically grows with (400) orientation preferentially to accommodate oxygen vacancies on these planes. Also, in the case of the sample deposited with 1.68 μm, it is assumed that recrystallization occurs, that is, the lattice structure rearranges at that thickness. Also, high sputtering energy,[30] high deposition temperature during sputtering,[31] or using oxygen-free electron cyclotron resonance sputtering[32] has been observed to be favourable for the growth of (400) oriented ITO films at 1.68 μm. Hence it is found that, ITO sample having 1.68 μm thicknesses is relatively well crystallized into cubic structure.

On the other hand, the XRD data of the ITO film deposited with 2.58 μm, showed single crystallinity as shown in Figure 1(f) with a sharp peak only for (440) orientation. The main reason for this is that when an ITO film deposits on the substrate, the accumulated particles build higher thickness.[33] Also, ITO films on the substrate appeared crystalline because of high energy particles[34] and the reduced oxygen vacancies with decreased carrier concentration[35] led to an increase in resistivity of the 2.58 μm thick sample.

As well, there seems some difference in crystal orientation and in particle size among the samples of different thickness.

XRD results indicate the four main different orientations (222), (400), (440) and (433) normally observed for ITO films.[36]

Via Scherrer's equation

$$D = \frac{0.9\lambda}{\beta\cos\theta} \tag{1}$$

Powder diffraction patterns can be used to calculate the average crystallite size. It is observed that average grain size increases from 10.5 nm to 34.4 nm with increasing film thickness from 0.84 μm to 2.58 μm (Fig. 2).

In the case of crystal orientation, the ratio of peak intensity originated from any of the (400), (440) and (622) peak divided
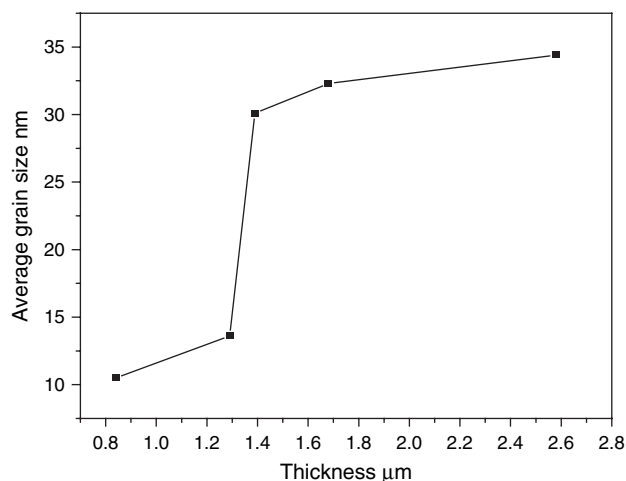
Table I. Microstructural parameters from XRD results of ITO thin films deposited with different thickness.

Micro structural parameters	Thickness				
	0.84 μm	1.29 μm	1.39 μm	1.68 μm	2.58 μm
D (nm)	10.5	13.6	30.1	32.3	34.40
L (nm)	12.0	65.0	6.39	126.2	16.05
D/L	0.88	0.21	4.71	0.26	2.14
I_{440} / I_{222}	2.82	0.19	0.45	0.05	—
Δa (nm)	4×10^{-3}	4.8×10^{-4}	4.2×10^{-3}	3.5×10^{-2}	2.2×10^{-3}

by that of (222) are considerably changed according to different thickness of ITO films. Therefore, we compared the crystal orientation by calculating the ratio.[37] The ratios of I_{440}/I_{222} of the samples having 0.84, 1.29, 1.39 and 1.68 μm thickness are 2.82, 0.19, 0.45 and 0.05 respectively (Table I). The ratios are highest at 0.84 μm (Fig. 3). It is guessed that it is attributed to the difference in O_2 concentration.[38] In the lattice structure of ITO films, (622) and (440) planes have more oxygen atoms than (222) plane.[38]

Moreover, all the ITO samples exhibit a larger lattice parameter than that of pure In_2O_3[39] giving additional evidence for the incorporation of Sn^{4+} into the indium oxide lattice (Table I). The increase of the lattice parameter is attributed to the larger repulsive forces arising from the additional positive charge of tin cations. To balance this extra charge, free electrons are released into the conduction band, increasing carrier concentration and consequently resulting in higher conductivity.[40]

Rietveld refinements were done for all the conditions and revealed that In^{3+} ion and Sn^{4+} ion show a strong preference for In_1 and In_2 octahedral site. This is in agreement with the other literature results on the cation ordering of multi oxide semiconductor. The maximum amount of Sn^{4+} upto certain percentage (power 250 W) occupies In_1 and In_2 site in the composition In_2O_3 to $In_{1.94}Sn_{0.06}O_3$.

The multi oxide semiconductor forms a solid solution over the entire range of Sn doping, but distorted the In/Sn_1 and In/Sn_2 lattice heavily (Fig. 4). The solid solution is discontinuous as

Fig. 2. Variation of average grain size of ITO thin films against thickness of ITO Films.
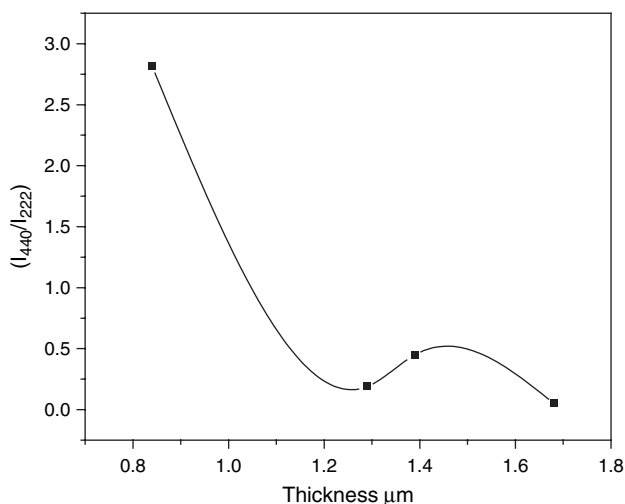
Fig. 3. A plot between I_{440}/I_{222} versus thickness of ITO thin films deposited by r.f sputtering.
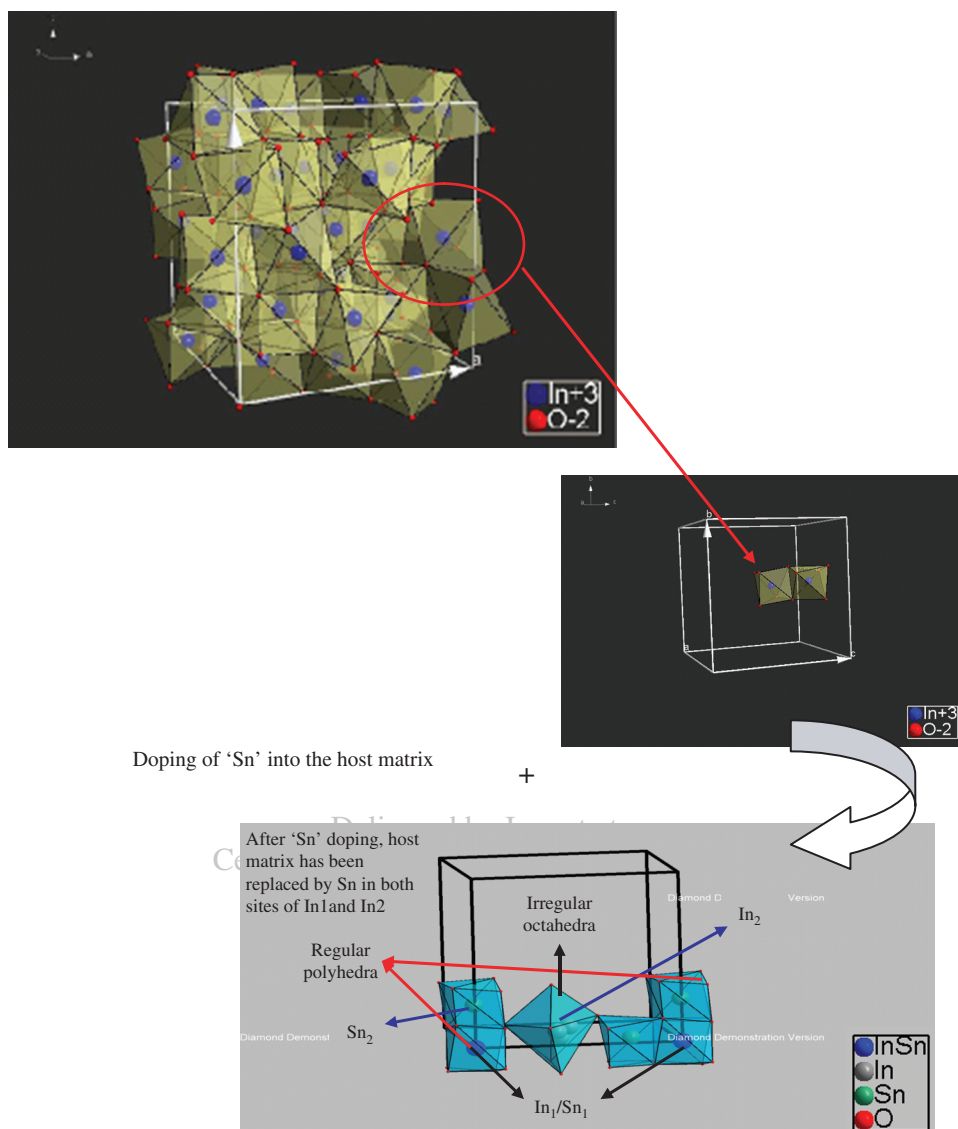
Fig. 4. Schematic representation of doping of Sn into In_2O_3 matrix. (a) In_2O_3 structure, (b) $Sn:In_2O_3$.

suggested by the deviation of the Vegard's law. The multi oxide semiconductor like $Sn:In_2O_3$ semiconductor has been intensively studied for the cation ordering for a long time. Studies on In_2O_3: Sn shows that larger cation In^{3+} (0.80A) preferentially occupied by Sn^{4+}(0.71 A) smaller (M_I and M_{II}) octahedral site. A similar cation ordering/ distortion are also observed in In_1 and In_2 by doping tin ions during preparation. The cation ordering in the multi oxide semiconductor is attributed to the covalent bonding provided by the d-orbital of the transition metal and the p-orbital of oxygen and to the crystal field stabilization energy (CFSE) with minor contribution.

3.2. TEM Analysis

Figure 5 shows the bright field image, selected area diffraction pattern and lattice fringe images of nanocrystalline ITO thin films. Particle agglomeration was observed and the particle size was determined to be 40(5) nm, consistent with the XRD results (Fig. 5(a)). The selected area diffraction pattern (SADP) shows that the major peaks correspond to ITO and the lattice

constants were consistent with the results obtained from XRD analysis (Fig. 5(a)-insert). The distance between the two lattice fringes was 1.00120 nm, corresponding to the (100) plane of ITO (Fig. 5(b)).
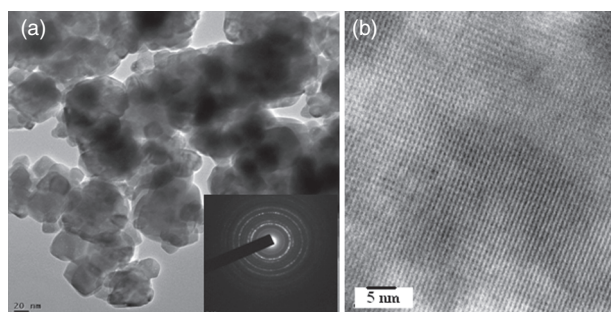
Fig. 5. TEM of 1.68 μm ITO thick film deposited by r.f sputtering: (a) Bright field image and (insert) selected area diffraction pattern, (b) HR TEM fringe pattern.
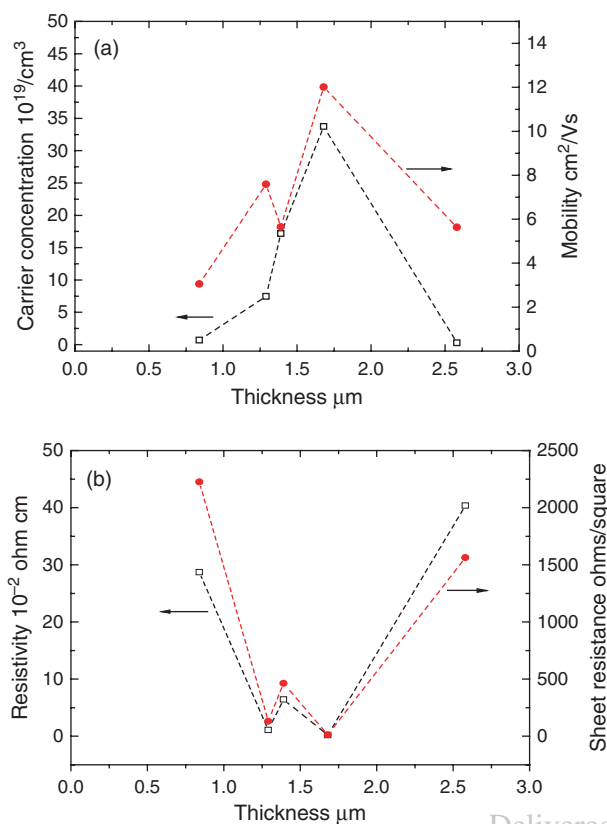
Fig. 6. Electrical properties of ITO thin films (a) carrier concentration and mobility of ITO films as a function of thickness (b) resistivity and sheet resistance of ITO films as a function of thickness.

3.3. Electrical Properties and Microstructure

Figures 6(a, b) show the variations of carrier concentration, mobility, resistivity and sheet resistance as function of thickness of ITO thin films prepared by r.f sputtering method. The lowest sheet resistance and the lowest resistivity are obtained at 1.68 μm and the corresponding values are found to be 12.36 Ω/square and 2.077×10^{-3} Ω cm respectively. The carrier concentration reaches a maximum value of 3.374×10^{20}/cm^{-3} and the carrier mobility reaches its highest value of 12.01 cm^2/Vs at 1.68 μm (Table II) as seen in Figure 6(b).

However, the causes for this type of mobility change versus thickness of ITO films become an issue that authors are interested in. On the other hand, XRD provides us with plenty of interesting information that reveals some correlation between mobility and microstructure. Moreover, for ITO films with such carrier concentration, they are degenerate semiconductor and the mean free path L of conduction electrons can be calculated using the

model of free electron Fermi gas.[41] That is,

$$L = \frac{3^{1/3}h}{(2\pi^{1/3}e^2\rho n^{2/3})} \qquad (2)$$

where h is the Planck's constant and e is the electron charge. Having D and L, the inside grain scattering effect of carriers for ITO films can be compared according to their D/L values. Calculation results of these XRD related data are shown in Table I. From the correlation of the data shown in Tables I and II, the causes for the mobility change may be given as follows. First, the mean free path of conduction electrons is larger than mean grain size for all films except for the films deposited with thicknesses of 1.39 μm and 2.58 μm. There are obviously different D/L values of about 0.88, 0.21, 4.71, 0.26 and 2.14 for these ITO films. ITO film deposited at 1.68 μm has the lowest D/L value of 0.26 and the mean free path of conduction electrons is the highest having relatively larger grains hence will experience fewer inside-grain scatterings than those of other samples with less grain boundary scatterings. Therefore, fewer inside-grain scatterings and negligible grain boundary scatterings are considered to be the reasons why ITO films deposited at 1.68 μm, has better electron mobility and hence, the scattering of conduction electrons inside the grain plays an important role in affecting the electron mobility. This crystallinity difference is most likely due to the difference in the bombarding energy of particle during film deposition.

Frank and Kostlin[42] found that at the same and high doping level, the lattice constant of oxidised ITO film is smaller than that of reduced ITO. The position of each XRD peak $(2\theta)_{440}$ is used to calculate the lattice constant 'a' of each of ITO film and the deviation from that of standard In$_2$O$_3$ (1.00118 nm), Δa (=$a - 1.0118$ nm), is obtained. A negative value of Δa means lattice contraction and a positive value means lattice expansion. The lattice constant change indicated by Δa value of our samples shows that all the samples have positive Δa. This indicates that they are in more reduced states, hence the sample deposited with a thickness of 1.68 μm, possesses greater value of Δa (+0.035 nm), can have higher electron mobility[43] of 12.01 cm^2/Vs. The sample deposited at 1.29 μm, possesses the smaller value of Δa (= +0.00048 nm), can have lesser electron mobility of about 7.587 cm^2/Vs.

3.4. Optical Investigations

The typical optical transmission T spectra of few representative ITO films on glass substrates are shown in Figure 7. The average transmission (T_{av}) of ITO films is defined in the visible wavelength region (400–800 nm) as $T_{av} = T_s/T_g$, where T_s is the mean transmission of sample (ITO/glass) and $T_g \sim 0.99$ is the measured mean transmission of glass.

The simultaneous achievement of maximum optical transmission and electrical conductivity is an important but not an easy

Table II. Electrical and optical properties of ITO films deposited with different thickness.

Thickness 'd' μm	n/cm^3	μ cm^2/Vs	P Ω cm	Sheet resistance Ω/square	Figure of Merit Ω^{-1}	Band Gap eV
0.84	7.119×10^{18}	3.055	2.870×10^{-1}	2224.8	3.7×10^{-4}	3.41
1.29	7.467×10^{19}	7.587	1.102×10^{-2}	131.2	6.3×10^{-3}	3.39
1.39	1.718×10^{20}	5.649	6.433×10^{-2}	462.8	1.8×10^{-3}	3.40
1.68	3.374×10^{20}	12.01	2.077×10^{-3}	12.36	6.5×10^{-2}	3.48
2.58	2.748×10^{18}	5.631	4.035×10^{-1}	1563.95	5.6×10^{-4}	3.36
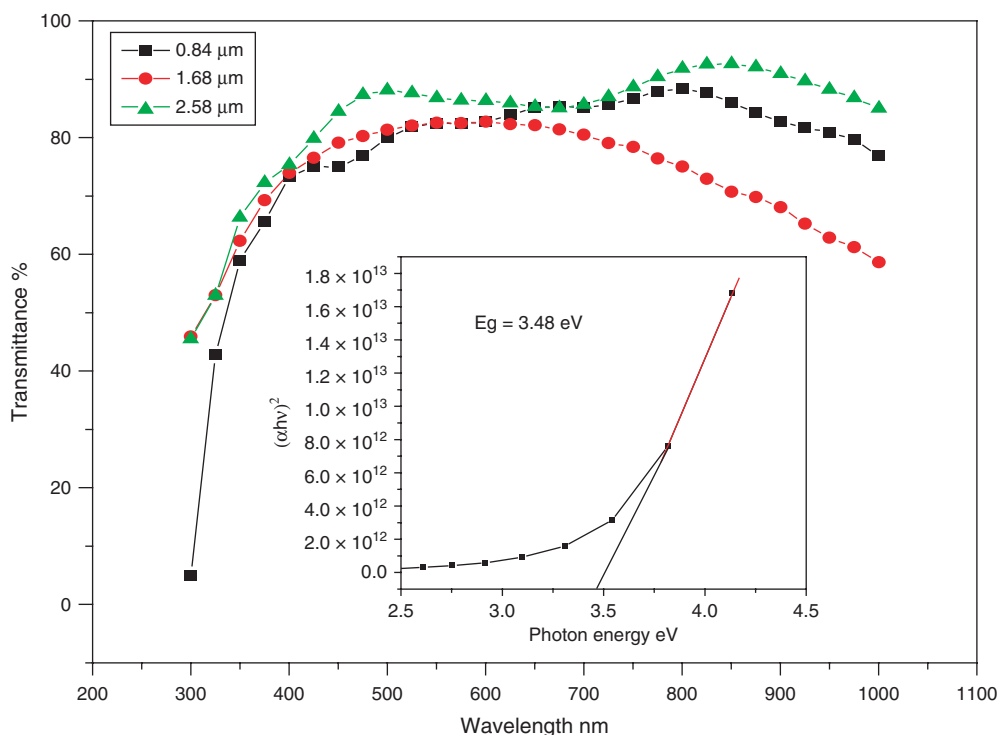
Fig. 7. Optical transmission T spectra of few representative ITO films deposited with different thickness. (Inset) Plot of Photon energy versus $(\alpha h\nu)^2$ for the ITO sample deposited with 1.68 μm thickness.

task since these two properties are inversely related. Therefore, a figure of merit has been developed to characterise transparent conductive oxide films like ITO. An optimal consideration between electrical sheet resistance R_s and optical transmission was suggested by Haacke[44] who defined the figure of merit as

$$\phi = T_{av}/R_s \qquad (3)$$

with the average transmittance, T_{av}, being computed in the 400–800 nm wavelength range. The optimal value is found to be 6.5×10^{-2} Ω^{-1}, achieved at 1.68 μm thickness at which the sample is with the maximum carrier concentration (Table II).

Refractive index and extinction coefficient values of ITO films in the wavelength range 350 nm to 1000 nm were calculated from the interference patterns of transmission spectra. Figure 8 shows the variation of refractive index and extinction coefficient with wavelength for the film deposited with 1.68 μm thicknesses. It shows a high refractive index value of 1.92 at 550 nm which is in agreement with the reported value of 1.86 for the ITO films deposited by reactive RF magnetron sputtering.[45] The average extinction coefficient value is about 0.067. It confirms

Fig. 8. Variation of refractive index and extinction coefficient with wavelength for the ITO film deposited with 1.68 μm thickness.
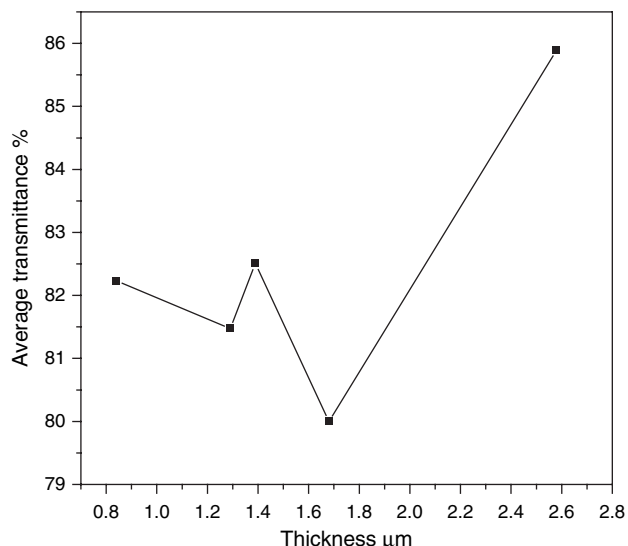
Fig. 9. Optical transmittance of the ITO thin films averaged over a wavelength range of 400–800 nm (visible) against thickness.

the formation of highly compact, void free and fully crystallized structure of the ITO films deposited at 1.68 μm thickness.

The transmittance data obtained for the films were used to calculate the absorption coefficients at different wavelengths using the following relation:

$$T = \exp(-\alpha d) \tag{4}$$

where d is the film thickness and T is the transmittance of the film. The optical band gap of the ITO films is calculated from the transmission spectra by assuming a parabolic band structure for the material. The relationship between the absorption coefficient and the optical band gap can be expressed as

$$\alpha h\nu = A(h\nu - E_g)^{1/N} \tag{5}$$

where E_g is the band gap energy, α is the absorption coefficient corresponding to frequency ν. The constant N depends on the nature of electronic transition. In the case of ITO films, N is equal to 2 for direct allowed transition. The optical band gaps
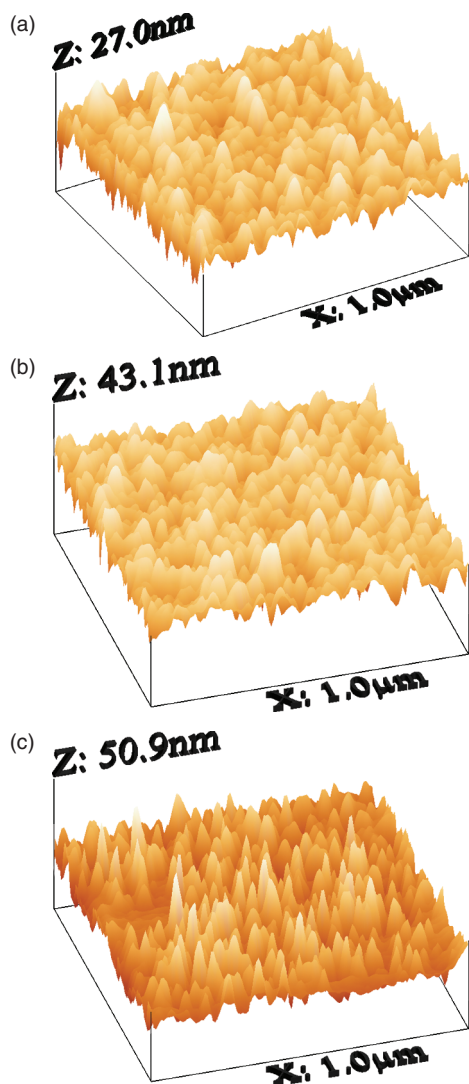
of ITO were determined[46] by extrapolating the linear portion of the curve from the plot of $(\alpha h\nu)^2$ versus $h\nu$ to $\alpha h\nu = 0$. In this study, the optical band gap values show a small variation between 3.36 and 3.48 eV, with the maximum band gap value of 3.48 eV for the 1.68 μm thick ITO film as observed from the inset of Figure 7. This value is smaller than the other reported values.[47, 48] The film thickness may be the reason for this low optical band gap value. The ITO films studied in this work are quite thick (approximately 1000 nm) and normally, the thicker the films is, the smaller the optical band gap is.[49] Also, the optical transmittance of the ITO thin films averaged over a wavelength range of 400 nm–800 nm (visible) plotted against thickness is shown in Figure 9. The average transmittance (80%) was obtained at 1.68 μm which also yielded the best structural and electrical properties.

3.5. Morphological Analysis by AFM

Figures 10(a, b and c) shows the three dimensional (3D) surface morphology of ITO films of thickness 2.58, 1.68 and 0.84 μm respectively. The increase in grain size with increasing thickness is evident from the surface topography. The grain size distribution of 1.68 μm thick ITO film is uniform and presents a smooth surface. The surface morphology for the 2.58 μm thick ITO films is non-uniform and is irregular with protrusions observed due to the larger sized grains above the small grains.

4. CONCLUSIONS

ITO films with thickness values ranging from 0.74 μm to 2.58 μm have been prepared by r.f. magnetron sputtering of a ceramic oxide target under Ar gas atmosphere. We have studied extensively the effect of thickness on the structural, optical and electrical properties. All these properties show a significant change at about 1.39 μm to 1.68 μm. The microstructure of the films is quite different for the thin and thick films. For thickness >1.29 μm, the films grow steadily with many grain orientations independent of the thickness, whereas for thickness <1.29 μm, there exist nearly only (222) and (400) orientations.

It can be concluded that the microstructure of the films changes with film growth, resulting in an improvement of the film's properties. Highly transparent ITO films with a visible transmittance of about 82% at 550 nm and a low resistivity of $2.077 \times 10^{-3} \Omega$ cm have been obtained at 1.68 μm thickness.

References and Notes

1. F. O. Adurodija, H. Izumi, T. Ishihara, H. Yoshioka, H. Matsui, and M. Motoyama, *Jpn. J. Appl. Phys.* 38, 2710 **(1999)**.
2. H. Kim, C. M. Gilmore, B. A. Pique, J. S. Horwitz, H. Mattoussi, H. Murata, Z. H. Kafafi, and D. B. Chrisey, *J. Appl. Phys.* 86 6451 **(1999)**.
3. C. Carvalho, Ph.D. Thesis, Faculdade de Ciencias e Technologia da Umoversodade Nova de Lis boa **(1995)**.
4. R. Groth, *Physics status Solidi.* 12, 69 **(1996)**.
5. R. Banerjee, D. Das, S. Ray, and A. Batabyal. *Sol. Energy Mater.* 13, 11 **(1985)**.
6. T. Karlson, A. Roos, and C. Ribbing, *Sol. Energy Mater.* 11, 469 **(1985)**.
7. G. Blandenet, Y. Iagarde, and J. Spitz, *Proc. 5th Int. Cof. on Chemical Vapour Deposition, Electrochemical Society.* **(1975)**, P. 170.
8. W. Molzen, *J. Vac. Sci. Technol.* 12, 99 **(1975)**.
9. J. Smith, A. Aronson, D. Chen, and W. Dass, *Thin Solid Films* 72, 469 **(1980)**.
10. E. Maruyama, S. Tsuda, and S. Nakano, Solid State Phenomena, Wiley, New York **(1995)**, Vol. 44, p. 863.
11. M. Powell, C. Glasse, I. French, A. Franklin, J. Hughes, and J. Curran, *Mater. Res. Soc. Symp.* 467, 863 **(1997)**.

Fig. 10. AFM of ITO thin films deposited by r.f sputtering with different thickness (a) 2.58 μm (b) 1.68 μm and (c) 0.84 μm.

12. R. Street, X. Wu, R. Weisfield, S. Ready, R. Apte, M. Nguyen, and P. Nylen, *Mater. Res. Soc. Symp*. 377, 757 **(1995)**.
13. J. Lan and J. Kanicki, *Mater. Res. Soc. Symp*. 424, 347 **(1997)**.
14. N. Harada, JARECT, *Amorphous Semiconductor Technologies & Devices* 16, 283 **(1984)**.
15. H. Kim, J. S. Horwitz, G. Kushto, A. Pique, Z. H. Kafafi, C. M. Gilmore, and D. B. Chrisey, *J. Appl. Phys*. 88 , 6021 **(2000)**.
16. A. Guittoum, L. Kerkache, and A. Layadi, *Eur. Phys. J*. 7, 201 **(1999)**.
17. P. K. Song, H. Akao, M. Kamei, Y. Shigesato, and I. Yasui, *Jpn. J. Appl. Phys*. 38, 5224 **(1999)**.
18. J. R. Bellingham, W. A. Phillips, and C. J. Adkins, *J. Phys. Condens. Matter*. 2, 6207 **(1990)**.
19. Powder diffraction file, Joint Committee on Powder diffraction Standards, ASTM, Philadelphia **(1976)**.
20. R. B. H. Tahar, T. Ban, Y. Ohya, and Y. Takahashi, *J. Appl. Phys*. 83, 2631 **(1998)**.
21. Y. Shigesato and D. C. Paine, *Appl. Phys. Lett*. 62, 1268 **(1993)**.
22. P. Sujatha Devi, M. Chatterjee, and D. Ganguli, *Mat. Lett*. 55, 205 **(2002)**.
23. A. K. Kakkarni, K. H. Schutz, T. S. Lin, and M. Khan, *Thin Solid Films*. 345, 273 **(1999)**.
24. Z. Qiao, R. Latz, and D. Mergel, *Thin Solid Films* 466, 250 **(2004)**.
25. Y. S. Jung, *Thin Solid Films* 467, 36 **(2004)**.
26. P. Thilakan, C. Minrari, S. Loreti, and E. Terzini, *Thin Solid Films* 388, 34 **(2001)**.
27. S. K. Choi and J. I. Lee, *J. Vac. Sci. Technol. A* 2043 **(2001)**.
28. H. Kim, J. S. Horwitz, G. Kushto, A. Pique, Z. H. Kafafi, C. M. Gilmore, and D. B. Chrisey, *J. Appl. Phys*. 88, 6021 **(2000)**.
29. G. Korotcenkov, V. Brinzari, A. Cerneavschi, M. Ivanov, V. Golovanov, A. Cornet, J. Morante, A. Cabot, and J. Arbiol, *Thin Solid Films* 460, 315 **(2004)**.
30. C. V. R. V. Kumar and A. Mansingh, *J. Appl. Phys*. 65, 1270 **(1989)**.

31. H. Kimura, H. Waranabe, S. Ishihara, Y. Suzuki, and T. Ito, *Shinku* 30, 546 **(1987)**, (in Japanese).
32. E. Kubota, J. Shigesaato, M. Igarashi, T. Haranou, K. Suzuki, *Jpn. J. Appl. Phys*. 33, 4997**(1994)**.
33. C. H. Yang, S. C. Lee, T. C. Lin, and S. Cheng, *Thin SolidFilms*. 516, 1984 **(2008)**.
34. M. T. Bhatti, A. M. Rama, and A. F. Khan, *Mater. Chem. Phys*. 84, 126 **(2004)**.
35. H. Kim, J. S. Horwitz, G. Kushto, A. Pique, Z. H. Kafafi, and C. M. Gilmore, *J. Appl. Phys*. 88 , 6021 **(2000)**.
36. C. Guillen, M. A. Martinez, Gutierrez, J. Herroro, H. A. Ossenbrink, P. Helm, H. E. hamnn (Eds.), Proceedings of the 14th *European Photovoltaic Solar energy Conference. Barcelona*, H. S. Stephens and Associates, Bedford, **(1997)**, p.1212.
37. N. C. Pramanik. S. Das, and P. K. Biswas, *Mat. Lett*. 56, 671 **(2002)**.
38. S.-J. Hong and J.-I. Han, *J. Electroceram* 17, 821 **(2006)**.
39. J. Ba, D. Fattakhova Rohlfing, A. Feldhoff, T. Brezesinski, I. Djerdj, M. Wark, and M. Niederberger, *Chem. Mater*. 18, 2848 **(2006)**.
40. H. Hwang, D. D. Edwards, D. R. Kammler, and T. O. Mason, *Solid State Ionics* 129, 135 **(2000)**.
41. C. Kittel, Introduction to Solid State Physics, 5th edn., John Wiley & Sons, Newyork **(1976)** p. 169.
42. G. Frank and H. Kostlin, *Appl. Phys A*. 27, 197 **(1982)**.
43. M. H. Yang, J. C. Wen, K. L. Chen, S. Y. Chen, and M. S. Leu, *Thin Solid Films* 484, 39 **(2005)**.
44. G. Haacke, *J. Appl. Phys*. 47, 4086 **(1976)**.
45. R. Das, K. Adhikary, and S. Ray, *Appl. Surf. Sci*. 253, 6068 **(2007)**.
46. M. T. Bhatti, A. M. Rana, and A. F. Khan, *Mater. Chem. Phys*. 84, 126 **(2004)**.
47. L.-J. Meng and M. P. Santos, *Thin Solid Films* 322, 56 **(1998)**.
48. J. Gearge and C. S. Menon, *Surf. Coat. Technol*. 132, 45 **(2000)**.
49. L.-J. M. P. Santos, *Vacuum*. 45, 1191 **(1994)**.